UNIVERSIDAD DE CONCEPCIÓN

Centro de Investigación en Ingeniería Matemática (CI^{2}MA)

Flux approximation on unfitted meshes and application to multiscale hybrid-mixed methods

Theophile Chaumont Frelet, Diego Paredes,
Frederic Valentin

PREPRINT 2023-02

SERIE DE PRE-PUBLICACIONES

FLUX APPROXIMATION ON UNFITTED MESHES AND APPLICATION TO MULTISCALE HYBRID-MIXED METHODS*

T. CHAUMONT-FRELET†, D. PAREDES‡, AND F. VALENTIN¶

Abstract. The flux variable determines the approximation quality of hybridization-based numerical methods. This work proves that approximating flux variables in discontinuous polynomial spaces from the L^2 orthogonal projection is super-convergent on meshes that are not necessarily aligned with jumping coefficient interfaces. The results assume only the local regularity of exact solutions in physical partitions. Based on the proposed flux approximation, we demonstrate that the mixed hybrid multiscale (MHM) finite element method is superconvergent on unfitted meshes, supporting the numerics presented in MHM seminal works.

1. Introduction

Many numerical algorithms rely on their accuracy in approximating flux variables defined on the skeleton of geometric partitions of physical domains. Finite volume methods, discontinuous finite element methods and hybrid finite element methods are examples of numerical methods of this type, but we also find the fundamental importance of flux recovery in some domain decomposition methods. As a result, there has been growing interest in developing discrete fluxes with optimal convergence properties (see [5], [17], [16], and [15] for instance).

In this work, we are interested in retrieving discrete fluxes associated with the solution u of partial differential equations defined in a domain Ω composed of regions ω where the regularity of the solution is high, although u can only have moderate overall regularity. We assume that the geometric partition $\mathcal{T}_{\mathcal{H}}$ of Ω used to define the discrete flux is general, with characteristic length $\mathcal{H}$, and composed of polytopal elements whose boundary may not fit on the interfaces of ω. Within such a scenario, we demonstrate that the exact flux λ can be accurately approximated through its L^2 orthogonal projection into a space $\Lambda_{H,\ell}$ of discontinuous piecewise polynomials of degree $\ell \geq 0$ on faces of $\partial\mathcal{T}_{\mathcal{H}}$ the boundary of $\mathcal{T}_{\mathcal{H}}$, notably,

$$\inf_{\mu_H \in \Lambda_{H,\ell}} \|\lambda - \mu_H\|_{\Lambda} = O(H^{\ell+3/2}),$$

* The second author was supported by Project EOLIS (MATH-AMSUD 21-MATH-04) and ANID-Chile through grant FONDECYT-1181572. The third author was partially supported by CNPq/Brazil No. 309173/2020-5 and FAPERJ E-26/201.182.2021, Project EOLIS (MATH-AMSUD 21-MATH-04) and Inria/France under the Inria International Chair.

†Centre Inria de l'Université Côte d'Azur, CNRS, LJAD, France

‡Departamento de Ingeniería Matemática and CI^{2}MA, Universidad de Concepción, Chile

¶LNCC - National Laboratory for Scientific Computing, Brazil and Centre Inria de l'Université Côte d'Azur, France

where H is a characteristic length associated to the discretization of $\partial\mathcal{T}_{\mathcal{H}}$. The norm $\|\cdot\|_{\Lambda}$ naturally appears in the analysis of hybridized methods and is rigorously introduced hereafter. Here, we understand a flux variable λ as the normal component of vector (tensor) functions $\boldsymbol{\sigma} \in \boldsymbol{H}(\mathrm{div}, \Omega)$ restricted to the skeleton of $\mathcal{T}_{\mathcal{H}}$. We have borrowed the term flux from fluid flows, although it may represent other physical quantities (e.g., traction in the elasticity model). This aim is similar to that found in the fictitious domain method [3] or in CutFEM [6], to name a few.

We take advantage of the proposed flux approximation to renew the analysis of the mixed hybrid multiscale method (MHM) on unfitted meshes. The MHM method was originally proposed in [12] and a priori and a posteriori error estimates proposed in [2], and extended to polygonal elements in [4] (see [14] for an abstract framework). It is conceived from the primal hybridization of the original model, and characterizes the exact solution in terms of a global formulation placed on the skeleton of a domain partition and independent local problems. Lagrange multipliers play the role of Neumann boundary conditions for local problems. Such decomposition leads to discretization, decouples global and local problems and gives rise to the MHM method. Regarding the analysis, and assuming that the local problems that define the multi-scale basis functions are exactly solved, we note that the original technique used to prove that the MHM method converges is fundamentally based on the accuracy of the approximation flux in a polynomial space $\Lambda_{H,\ell}$ of degree ℓ on the boundary partition (see [8] for a recent alternative proof). Specifically, if u_H denotes the MHM solution, the convergence of u_H toward u in the (broken) Sobolev norm behaves as follows (c.f. [2]): for $0 \leq q \leq \ell$, we have

$$\|\boldsymbol{\nabla}(u - u_H)\|_{\mathcal{T}_{\mathcal{H}}} \leq C_\ell \inf_{\mu_H \in \Lambda_{H,\ell}} \|\lambda - \mu_H\|_{\Lambda} \leq C_\ell H^{q+1} |u|_{H^{q+2}(\mathcal{T}_{\mathcal{H}})},$$

where C_ℓ is a positive constant depending on ℓ. We note that the above estimate depends on the regularity of the exact solution placed on the geometric partition of Ω rather than the physical partition. Also, the constant depends on the degree of the polynomial, but lacks its precise dependence, which is important for establishing convergence with respect to ℓ.

Therefore, in addition to the proposed discrete fluxes in general unfitted meshes, this work fills the gap in the original numerical analysis of the MHM method. In particular we (i) demonstrate that the MHM method is superconvergent. Specifically, the convergence rate of $\|\boldsymbol{\nabla}(u - u_H)\|_{\mathcal{T}_{\mathcal{H}}}$ behaves like $O(H^{\ell+3/2})$ when $H \to 0$ (and $\mathcal{H}$ stay fixed), which was numerically anticipated in [13] and [4], (ii) prove that the MHM method achieves convergence in unfitted meshes assuming local regularity in the physical domain unlike the previous MHM literature and (iii) explicit the dependence of the constant on the error estimates in the polynomial degree ℓ. We show that the MHM method converges optimally when $\ell \to \infty$. Such a convergence result is also new.

The outline of this article is as follows: Section 2 provides the functional setting given in an abstract form to be particularized in the next sections. Section 3 includes a description of the physical partition and the mesh, followed by the definition of broken spaces and associated norms. In Section 4, we introduce our new flux interpolation operator and

establish error estimates. These error estimates are used in Section 5 to revisit the analysis of the MHM method. Section 6 is devoted to numerical illustrations, and concluding remarks follow in Section 7.

2. Functional setting and norms

If $\mathcal{U} \subset \Omega$ is a measurable set, $L^2(\mathcal{U})$ is the usual Lebesgue space of square-integrable functions, equipped with its inner product $(\cdot,\cdot)_{\mathcal{U}}$ and the associated norm $\|\cdot\|_{\mathcal{U}}^2 := (\cdot,\cdot)_{\mathcal{U}}$. We also employ the notation $\boldsymbol{L}^2(\mathcal{U}) := [L^2(\mathcal{U})]^d$, and we keep the same notation for its inner product and norm. For $m \in \mathbb{N}^\star$, $H^m(\mathcal{U})$ is the usual Sobolev space that we equip with the norm

$$\|v\|_{H^m(\mathcal{U})}^2 := \sum_{\substack{\boldsymbol{\alpha}\in\mathbb{N}^d \\ |\boldsymbol{\alpha}|\le m}} \left(\frac{1}{d_{\mathcal{U}}^2}\right)^{m-|\boldsymbol{\alpha}|} \|\partial^{\boldsymbol{\alpha}} v\|_{\mathcal{U}}^2$$

and semi-norm

$$|v|_{H^m(\mathcal{U})}^2 := \sum_{\substack{\boldsymbol{\alpha}\in\mathbb{N}^d \\ |\boldsymbol{\alpha}|= m}} \|\partial^{\boldsymbol{\alpha}} v\|_{\mathcal{U}}^2$$

for all $v \in H^m(\mathcal{U})$, where $d_{\mathcal{U}}$ is the diameter of $\mathcal{U}$ and the the partial derivative $\partial^{\boldsymbol{\alpha}}$ is understood in the sense of distributions. We refer the reader to [1] for an in-depth discussion of these spaces. We shall also use the Sobolev space $\boldsymbol{H}(\mathrm{div},\mathcal{U})$ of functions $\boldsymbol{w} \in \boldsymbol{L}^2(\mathcal{U})$ with $\boldsymbol{\nabla}\cdot\boldsymbol{w} \in L^2(\mathcal{U})$, see [11].

We write $H^{1/2}(\partial\mathcal{U})$ for the image of $H^1(\mathcal{U})$ by the trace operator. Its dual, that we denote by $H^{-1/2}(\partial\mathcal{U})$, is the image of $\boldsymbol{H}(\mathrm{div},\mathcal{U})$ by the normal trace operator, and we reserve the notation $\langle\cdot,\cdot\rangle_{\partial\mathcal{U}}$ for the duality pairing between $H^{-1/2}(\partial\mathcal{U})$ and $H^{1/2}(\partial\mathcal{U})$.

If $\mathcal{P}$ is a collection of non-overlapping measurable sets, we introduce for $m \in \mathbb{N}^\star$ the broken Sobolev space

$$H^m(\mathcal{P}) := \left\{ v \in L^2(\Omega) \mid v|_\omega \in H^m(\omega)\ \forall \omega \in \mathcal{P} \right\},$$

with its norm and semi-norm

$$\|v\|_{H^m(\mathcal{P})}^2 := \sum_{\omega\in\mathcal{P}} \|v\|_{H^m(\omega)}^2 \quad \text{and} \quad |v|_{H^m(\mathcal{P})}^2 := \sum_{\omega\in\mathcal{P}} |v|_{H^m(\omega)}^2 \quad \forall v \in H^m(\mathcal{P}).$$

If $\mathcal{V} \subset \Omega$ is contained in an hyperplane and measurable with respect to the surface measure, we employ the same notations as above for $L^2(\mathcal{V})$ its norm and inner-product, with integration performed with respect to the surface measure. $H^m(\mathcal{V})$ is also defined likewise, with multi-indices running over $\mathbb{N}^{d-1}$. Finally, if $\mathcal{Q}$ is a collection of such disjoint sets $\mathcal{V}$, then $H^m(\mathcal{Q})$ is the associated broken Sobolev space. We will also need the (possibly infinite) Sobolev-Slobodeckij semi-norm

$$|v|_{H^{1/2}(\mathcal{V})}^2 := \int_{\mathcal{V}}\int_{\mathcal{V}} \frac{|v(\boldsymbol{x}) - v(\boldsymbol{y})|^2}{|\boldsymbol{x}-\boldsymbol{y}|^d} d\boldsymbol{y} d\boldsymbol{x} \qquad \forall v \in L^2(\mathcal{V}),$$

and its piecewise version

$$|v|^2_{H^{1/2}(\mathcal{Q})} := \sum_{\mathcal{V}\in\mathcal{Q}} |v|^2_{H^{1/2}(\mathcal{V})} \qquad \forall v \in L^2(\mathcal{Q}).$$

Consider an affine subspace $\mathcal{Z}^r$ of $\mathbb{R}^d$ of dimension $(d-1) \le r \le d$ (i.e. an hyperplane or the whole $\mathbb{R}^d$), and a closed connected subset $U \subset \mathcal{Z}^r$ with non-empty interior. We denote by h_U the diameter of the smallest ball containing U, and by ρ_U the diameter of the largest ball B such that U is star-shaped with respect to B. We also denote by $\mathcal{F}_U$ the set of "faces" of U. Then, the shape-regularity parameter of U is the constant

$$\beta_U := \frac{h_U}{\rho_U}.$$

There exist $\boldsymbol{a}, \boldsymbol{u}^{(j)} \in \mathbb{R}^d$ and functions $y_j : \mathcal{Z}^r \to \mathbb{R}$ such that

$$\boldsymbol{x} = \boldsymbol{a} + \sum_{j=1}^{r} y_j(\boldsymbol{x})\boldsymbol{u}^{(j)} \qquad \forall \boldsymbol{x} \in \mathcal{Z}^r.$$

Then, for $\ell \in \mathbb{N}$ the space $\mathbb{P}_\ell(U)$ of polynomials of degree ℓ on U collects all the functions $v : U \to \mathbb{R}$ of the form

$$v = \sum_{\substack{\boldsymbol{\alpha}\in\mathbb{N}^r \\ |\boldsymbol{\alpha}|_2\le\ell}} v_{\boldsymbol{\alpha}} \prod_{j=1}^{r} y_j^{\boldsymbol{\alpha}_j},$$

where each $v_{\boldsymbol{\alpha}} \in \mathbb{R}$.

When considering a collection $\mathcal{C} := \{U_1, \dots, U_n\}$ of disjoint affine sets as described above, we let $\beta_{\mathcal{C}} := \max_{1\le j\le n} \beta_{U_j}$, and $\mathbb{P}_\ell(\mathcal{C})$ stands for the set of functions $v : \cup_{j=1}^n U_j \to \mathbb{R}$ such that $v|_{U_j} \in \mathbb{P}_\ell(U_j)$ for $1 \le j \le n$.

3. Partitions of the Domain

We consider a Lipschitz polytopal domain $\Omega \subset \mathbb{R}^d$, with $d \in \{2, 3\}$, and denote by d_Ω the diameter of Ω. The domain Ω is decomposed into two separate and independent partitions. They are detailed next.

3.1. Physical partition.

We assume that Ω is partitioned into "physical subdomains" $\omega \in \mathcal{P}_\Omega$. We will assume that each ω has a Lipschitz boundary. As a result [20, Theorem 5, Page 181], there exists extension operators $E_\omega : L^2(\omega) \to L^2(\Omega)$ satisfying $(E_\omega v) = v$ for all $v \in L^2(\Omega)$ and such that, for all $m \in \mathbb{N}$, $E_\omega : H^m(\omega) \to H^m(\Omega)$ with

$$\|E_\omega v\|_{m,\Omega} \le C_{\mathrm{E},\omega,m}\|v\|_{m,\omega}$$

for all $v \in H^m(\omega)$ for some constants $C_{\mathrm{E},\omega,m}$, and we set $C_{\mathrm{E},\mathcal{P}_\Omega,m} := \max_{\omega\in\mathcal{P}_\Omega} C_{\mathrm{E},\omega,m}$. This physical partition typically corresponds to regions of space occupied by different materials, each being linked with a constant (or smooth) coefficient in the considered model problem (more in Section 5). Importantly, we may expect the model's solution to be smooth in each of the physical subdomains $\omega \in \mathcal{P}_\Omega$.

3.2. **Geometrical partitions.** We further partition the domain into a computational mesh $\mathcal{T}_\mathcal{H}$ characterized by a size $\mathcal{H} > 0$. This partition is made of polytopal regions K, and we collect the element boundaries ∂K in the set $\partial\mathcal{T}_\mathcal{H}$. We denote by $\mathcal{F}_\mathcal{H}$ the faces of partition $\mathcal{T}_\mathcal{H}$, and for $K \in \mathcal{T}_\mathcal{H}$, $\mathcal{F}_K$ is the set of faces of K. For the sake of simplicity, we assume that for two distinct regions $K_+, K_- \in \mathcal{T}_\mathcal{H}$, that when intersection $\partial K_+ \cap \partial K_-$ is non-empty, it is either a full face, a full edge, or a single vertex of both regions. We highlight that we *do not* assume any conformity between the partition $\mathcal{T}_\mathcal{H}$ with the physical partition $\mathcal{P}_\Omega$.

We denote by $C_{\mathrm{qu}}(\mathcal{T}_\mathcal{H})$ the quasi-uniformity constant of $\mathcal{T}_\mathcal{H}$, i.e., the smallest real number such that

$$\mathcal{H} \le C_{\mathrm{qu}}(\mathcal{T}_\mathcal{H})\mathcal{H}_K \qquad \forall K \in \mathcal{T}_\mathcal{H}.$$

Then, for each $K \in \mathcal{T}_\mathcal{H}$, there exists a constant $C_{\mathrm{tr},K}$ solely depending on β_K and $C_{\mathrm{qu}}(\mathcal{T}_\mathcal{H})$ such that

$$\|v\|_{\mathcal{F}_K}^2 \le C_{\mathrm{tr},K}^2 \left(\mathcal{H}^{-1}\|v\|_K^2 + \mathcal{H}\|\boldsymbol{\nabla} v\|_K^2\right) \tag{3.1}$$

and

$$|v|_{H^{1/2}(\mathcal{F}_K)} \le C_{\mathrm{tr},K}\|\boldsymbol{\nabla} v\|_K \tag{3.2}$$

for all $v \in H^1(K)$, see, e.g., [10, Lemmas 6.1 and 6.4]. We write $C_{\mathrm{tr},\mathcal{T}_\mathcal{H}} := \max_{K\in\mathcal{T}_\mathcal{H}} C_{\mathrm{tr},K}$, which only depends on $\beta_{\mathcal{T}_\mathcal{H}}$ and $C_{\mathrm{qu}}(\mathcal{T}_\mathcal{H})$. Notice that because $C_{\mathrm{qu}}(\mathcal{T}_\mathcal{H})$ enters our analysis, our results are essentially relevant on quasi-uniform meshes where the ratio between the maximal and minimal element diameter is not large.

The following space of element-wise zero mean value functions

$$\mathbb{P}_0^\perp(\mathcal{T}_\mathcal{H}) := \left\{v \in H^1(\mathcal{T}_\mathcal{H}) \mid (v, q_0)_{\mathcal{T}_\mathcal{H}} = 0 \ \forall q_0 \in \mathbb{P}_0(\mathcal{T}_\mathcal{H})\right\},$$

will be useful.

We further introduce another level of geometrical discretization. Namely, each face $F \in \mathcal{F}_\mathcal{H}$ is partitioned into a mesh $\mathcal{M}_H^F$ with elements D and characteristic length H. For $0 \le q \le \ell$, and $\ell \ge 0$, the orthogonal projector $\pi_{D,\ell} : L^2(D) \to \mathbb{P}_\ell(D)$ satisfies

$$\|\xi - \pi_{D,\ell}\xi\|_D \le \left(\frac{C_{\mathrm{P},D,q}H_D}{\ell+1}\right)^{q+1} |\xi|_{H^{q+1}(D)} \qquad \forall \xi \in H^{q+1}(D), \tag{3.3}$$

where $C_{\mathrm{P},D,q}$ only depends on the shape of D, and not on its size. Upper bounds for $C_{\mathrm{P},D,q}$ expressed in terms of the geometrical features of D are listed in Remark 3.1. In addition, using Banach space interpolation theory (see, e.g. [21, Chapters 22, 34 and 36]), we can combine the case $q = 0$ and $q = 1$ of (3.3) to show that

$$\|\xi - \pi_{D,\ell}\xi\|_D \le \left(\frac{C_{\mathrm{P},D,\mathrm{h}}H_D}{\ell+1}\right)^{1/2} |\xi|_{H^{1/2}(D)} \quad \forall \xi \in H^{1/2}(D), \tag{3.4}$$

for some constant $C_{\mathrm{P},D,\mathrm{h}}$ only depending on the shape of D. We denote by $\mathcal{M}_H := \cup_{F\in\mathcal{F}_\mathcal{H}}\mathcal{M}_H^F$ the global skeletal mesh, and we set

$$C_{\mathrm{P},\mathcal{M}_H,q} := \max_{F\in\mathcal{F}_\mathcal{H}} \max_{D\in\mathcal{M}_H^F} C_{\mathrm{P},D,q}, \qquad C_{\mathrm{P},\mathcal{M}_H,\mathrm{h}} := \max_{F\in\mathcal{F}_\mathcal{H}} \max_{D\in\mathcal{M}_H^F} C_{\mathrm{P},D,\mathrm{h}}.$$

We also set $\mathcal{M}_H^{\partial K} := \cup_{F\in\mathcal{F}_K}\mathcal{M}_H^F$ for each $K \in \mathcal{T}_\mathcal{H}$ and $\mathcal{M}_H^\omega := \{D \in \mathcal{M}_H \mid D \subset \omega\}$.

In contrast to $\mathcal{T}_\mathcal{H}$, we assume that the partition $\mathcal{M}_H$ fits the physical partition $\mathcal{P}_\Omega$. It means that every element $D \in \mathcal{M}_H$ entirely belongs to a single physical subdomain $\omega \in \mathcal{P}_\Omega$. Notice that we do not assume that the elements $D \in \mathcal{M}_H$ are polygons, so that curved boundaries are allowed.

Remark 3.1 (Projection constants)**.** *When $d = 2$, the elements $D \in \mathcal{M}_H$ correspond to segments, so there is only one possible shape and one constant $C_{\mathrm{P},D,q}$. When $d = 3$, several formulas giving explicit upper bound for $C_{\mathrm{P},D,q}$ in terms of its geometrical characteristics are available in the literature. For instance, if D is a polygon, it follows from* [9, Lemma 4.2 and Remark 2] *that it only depends on β_D, q and the ratio $h_D/\min_{e\in\mathcal{F}_D} h_e$ (the h_e denoting the lengths of the edges of D). We note, however, that the result in* [9] *are designed for virtual element interpolation operators, whereas we need a projection without compatibility constraints. As a result, the dependence on $C_{\mathrm{P},D,q}$ on $h_D/\min_{e\in\mathcal{F}_D} h_e$ may be suboptimal. Indeed, a careful inspection of* [7, Lemma 23] *shows that the key parameter is the continuity constant of Stein's extension operator $H^q(D) \to H^q(\mathbb{R}^{d-1})$. For the sake of simplicity, we do not pursue such a detailed analysis here.*

4. Flux interpolation

This section presents our first set of results, where we construct an interpolation operator for flux variables and establish associated error estimates.

4.1. Continuous and discrete fluxes.

We consider that the continuous flux variable belongs to the space

$$\Lambda(\partial\mathcal{T}_\mathcal{H}) := \left\{ \mu \in \prod_{K\in\mathcal{T}_\mathcal{H}} H^{-1/2}(\partial K) \;\middle|\; \begin{array}{l} \exists \boldsymbol{\sigma} \in \boldsymbol{H}(\mathrm{div},\Omega); \\ \boldsymbol{\sigma}\cdot\boldsymbol{n}_K = \mu|_{\partial K}\ \forall K \in \mathcal{T}_\mathcal{H} \end{array} \right\}.$$

If $\mu \in \Lambda(\partial\mathcal{T}_\mathcal{H})$ and $v \in H^1(\mathcal{T}_\mathcal{H})$, we define the pairing

$$\langle \mu, v\rangle_{\partial\mathcal{T}_\mathcal{H}} = \sum_{K\in\mathcal{T}_\mathcal{H}} \langle \mu, v\rangle_{\partial K}.$$

For $\mu \in \Lambda(\partial\mathcal{T}_\mathcal{H})$, we define the (semi) norm

$$\|\mu\|_\Lambda = \sup_{\substack{v\in\mathbb{P}_0^\perp(\mathcal{T}_\mathcal{H}) \\ \|\boldsymbol{\nabla} v\|_{\mathcal{T}_\mathcal{H}}=1}} \langle \mu, v\rangle_{\partial\mathcal{T}_\mathcal{H}}. \tag{4.1}$$

Notice that $\|\cdot\|_\Lambda$ becomes a norm when restricted to the subspace of elements $\mu \in \Lambda$ such that $\langle \mu, v_0\rangle_{\partial\mathcal{T}_\mathcal{H}} = 0$ for all $v_0 \in \mathbb{P}_0(\mathcal{T}_\mathcal{H})$.

For a given integer $\ell \in \mathbb{N}$, we introduce an interpolation operator that is well defined for all $\mu \in \Lambda \cap L^2(\partial\mathcal{T}_\mathcal{H})$ by setting

$$(\pi_{H,\ell}\mu)|_D = \pi_{D,\ell}\mu \qquad \forall D \in \mathcal{M}_H$$

and it follows that the discrete flux $\pi_{H,\ell}\mu \in \Lambda(\mathcal{T}_\mathcal{H}) \cap L^2(\partial\mathcal{T}_\mathcal{H})$.

4.2. **Error estimates.** We start with a duality result that is similar to [3].

Lemma 4.1 (Duality). *For all $\mu \in \Lambda(\partial\mathcal{T}_\mathcal{H}) \cap L^2(\partial\mathcal{T}_\mathcal{H})$, we have*

$$\|\mu - \pi_{H,\ell}\mu\|_\Lambda \leq C_{\mathrm{tr},\mathcal{T}_\mathcal{H}} \left(\frac{C_{\mathrm{P},\mathcal{M}_H,\mathrm{h}} H}{\ell+1}\right)^{1/2} \|\mu - \pi_{H,\ell}\mu\|_{\partial\mathcal{T}_\mathcal{H}}. \tag{4.2}$$

Proof. Let $v \in H^1(\mathcal{T}_\mathcal{H})$. For all $K \in \mathcal{T}_\mathcal{H}$, we have

$$\langle \mu - \pi_{H,\ell}\mu, v\rangle_{\partial K} = (\mu - \pi_{H,\ell}\mu, v)_{\partial K} = \sum_{D \in \mathcal{M}_H^{\partial K}} (\mu - \pi_{D,\ell}\mu, v)_D.$$

Recalling that $\pi_{H,\ell}^D\mu$ is the $L^2(D)$ projection of μ onto $\mathbb{P}_\ell(D)$, and using (3.4), we have

$$\begin{aligned}(\mu - \pi_{D,\ell}\mu, v)_D = (\mu - \pi_{D,\ell}\mu, v - \pi_{D,\ell}v)_D &\leq \|\mu - \pi_{D,\ell}\mu\|_D \|v - \pi_{D,\ell}v\|_D \\ &\leq \left(\frac{C_{\mathrm{P},D,\mathrm{h}} H_D}{\ell+1}\right)^{1/2} \|\mu - \pi_{D,\ell}\mu\|_D |v|_{H^{1/2}(D)},\end{aligned}$$

and therefore, involving (3.2), we obtain

$$\begin{aligned}\langle \mu - \pi_{H,\ell}\mu, v\rangle_{\partial K} &\leq \left(\frac{C_{\mathrm{P},\mathcal{M}_H,\mathrm{h}} H}{\ell+1}\right)^{1/2} \|\mu - \pi_{H,\ell}\mu\|_{\mathcal{F}_K} |v|_{H^{1/2}(\mathcal{F}_K)} \\ &\leq C_{\mathrm{tr},\mathcal{T}_\mathcal{H}} \left(\frac{C_{\mathrm{P},\mathcal{M}_H,\mathrm{h}} H}{\ell+1}\right)^{1/2} \|\mu - \pi_{H,\ell}\mu\|_{\mathcal{F}_K} \|\boldsymbol{\nabla} v\|_K.\end{aligned}$$

By summation, we see that

$$\langle \mu - \pi_{H,\ell}\mu, v\rangle_{\partial\mathcal{T}_\mathcal{H}} \leq C_{\mathrm{tr},\mathcal{T}_\mathcal{H}} \left(\frac{C_{\mathrm{P},\mathcal{M}_H,\mathrm{h}} H}{\ell+1}\right)^{1/2} \|\mu - \pi_{H,\ell}\mu\|_{\partial\mathcal{T}_\mathcal{H}} \|\boldsymbol{\nabla} v\|_{\mathcal{T}_\mathcal{H}}$$

for all $v \in H^1(\mathcal{T}_\mathcal{H})$, and (4.2) follows by definition (4.1) of $\|\cdot\|_\Lambda$. □

As a direct consequence of Lemma 4.1 and (3.3), we have the following result.

Corollary 4.2 (Approximation). *Let $0 \leq q \leq \ell$. Assuming $\mu \in \Lambda(\partial\mathcal{T}_\mathcal{H}) \cap H^{q+1}(\partial\mathcal{T}_\mathcal{H})$, it holds*

$$\|\mu - \pi_{H,\ell}\mu\|_\Lambda \leq C_{\mathrm{tr},\mathcal{T}_\mathcal{H}} \left(\frac{C_{\mathrm{A},\mathcal{M}_H,q} H}{\ell+1}\right)^{q+3/2} |\mu|_{H^{q+1}(\mathcal{M}_H)}, \tag{4.3}$$

where $C_{\mathrm{A},\mathcal{M}_H,q} := \max(C_{\mathrm{P},\mathcal{M}_H,\mathrm{h}}, C_{\mathrm{P},\mathcal{M}_H,q})$.

In practical application, the variable $\lambda \in \Lambda(\partial\mathcal{T}_\mathcal{H})$ to be approximated is related to the "flux" of the solution u to the model problem under consideration. For instance, $\lambda|_{\partial K} = \boldsymbol{\nabla} u \cdot \boldsymbol{n}_K$ for the Laplace operator. This motivates the main result of this section.

Theorem 4.3 (Interpolation error estimate). *Let $0 \leq q \leq \ell$ and $\mu \in \Lambda(\partial\mathcal{T}_\mathcal{H}) \cap H^{q+1}(\partial\mathcal{T}_\mathcal{H})$. Assume that there exists $u \in H^{q+3}(\mathcal{P}_\Omega)$ such that*

$$|\mu|_{H^{q+1}(\mathcal{M}_H)} \leq |u|_{H^{q+2}(\mathcal{M}_H)}.$$

Then, we have

$$\|\mu - \pi_{H,\ell}\mu\|_\Lambda \leq C_{\mathrm{E},\mathcal{P}_\Omega,q+3} C_{\mathrm{tr},\mathcal{T}_\mathcal{H}} \left(\frac{C_{\mathrm{A},\mathcal{M}_H,q} H}{\ell+1}\right)^{q+3/2} \left(\mathcal{H}^{-1/2}\|u\|_{H^{q+2}(\mathcal{P}_\Omega)} + \mathcal{H}^{1/2}\|u\|_{H^{q+3}(\mathcal{P}_\Omega)}\right). \tag{4.4}$$

Proof. In view of (4.3), it is sufficient to establish that

$$|u|_{H^{q+2}(\mathcal{M}_H)} \leq C_{\mathrm{E},\mathcal{P}_\Omega,q+3} C_{\mathrm{tr},\mathcal{T}_\mathcal{H}} \left(\mathcal{H}^{-1/2}\|u\|_{H^{q+2}(\mathcal{P}_\Omega)} + \mathcal{H}^{1/2}\|u\|_{H^{q+3}(\mathcal{P}_\Omega)}\right).$$

First, because the mesh $\mathcal{M}_H$ fits the physical partition $\mathcal{P}_\Omega$, we have

$$\begin{aligned} |u|^2_{H^{q+2}(\mathcal{M}_H)} = \sum_{D\in\mathcal{M}_H} |u|^2_{H^{q+2}(D)} &\leq \sum_{\omega\in\mathcal{P}_\Omega} \sum_{D\in\mathcal{M}_H^\omega} |u|^2_{H^{q+2}(D)} \\ &= \sum_{\omega\in\mathcal{P}_\Omega} \sum_{D\in\mathcal{M}_H^\omega} \|E_\omega u\|^2_{H^{q+2}(D)} \leq \sum_{\omega\in\mathcal{P}_\Omega} \|E_\omega u\|^2_{H^{q+2}(\partial\mathcal{T}_\mathcal{H})}. \end{aligned}$$

On the other hand, for $K \in \mathcal{T}_\mathcal{H}$, we can apply (3.1) to $\partial^\alpha(E_\omega u)$ for $|\alpha| \leq q+2$. It follows that

$$\|E_\omega u\|^2_{H^{q+2}(\partial K)} \leq C^2_{\mathrm{tr},K}\left(\mathcal{H}^{-1}\|E_\omega u\|^2_{H^{q+2}(K)} + \mathcal{H}\|E_\omega u\|^2_{H^{q+3}(K)}\right),$$

and therefore

$$\begin{aligned} \|E_\omega u\|^2_{H^{q+2}(\partial\mathcal{T}_\mathcal{H})} &\leq C^2_{\mathrm{tr},\mathcal{T}_\mathcal{H}}\left(\mathcal{H}^{-1}\|E_\omega u\|^2_{H^{q+2}(\Omega)} + \mathcal{H}\|E_\omega u\|^2_{H^{q+3}(\Omega)}\right) \\ &\leq C^2_{\mathrm{E},\mathcal{P}_\Omega,q+3} C^2_{\mathrm{tr},\mathcal{T}_\mathcal{H}}\left(\mathcal{H}^{-1}\|u\|^2_{H^{q+2}(\omega)} + \mathcal{H}\|u\|^2_{H^{q+3}(\omega)}\right), \end{aligned}$$

for all $\omega \in \mathcal{P}_\Omega$. By summation over $\omega \in \mathcal{P}_\Omega$, it follows that

$$|u|^2_{H^{q+2}(\mathcal{M}_H)} \leq C^2_{\mathrm{E},\mathcal{P}_\Omega,q+3} C^2_{\mathrm{tr},\mathcal{T}_\mathcal{H}}\left(\mathcal{H}^{-1}\|u\|^2_{H^{q+2}(\mathcal{P}_\Omega)} + \mathcal{H}\|u\|^2_{H^{q+3}(\mathcal{P}_\Omega)}\right).$$

□

We close this section with an important property of our interpolation operator previously observed in [4].

Proposition 4.4 (Mass conservation)**.** *Assume that $\lambda \in \Lambda(\partial\mathcal{T}_\mathcal{H}) \cap L^2(\partial\mathcal{T}_\mathcal{H})$. Then, we have*

$$\langle \pi_{\ell,H}\lambda, v_0\rangle_{\partial\mathcal{T}_\mathcal{H}} = \langle \lambda, v_0\rangle_{\partial\mathcal{T}_\mathcal{H}} \quad \forall v_0 \in \mathbb{P}_0(\mathcal{T}_\mathcal{H}). \tag{4.5}$$

Proof. Since λ (and $\pi_{\ell,H}\lambda$) belongs to $L^2(\partial\mathcal{T}_\mathcal{H})$ by assumption, we can regroup the duality pairings into face-by-face L^2 products, leading to

$$\langle \lambda - \pi_{H,\ell}\lambda, v_0\rangle_{\partial\mathcal{T}_\mathcal{H}} = \sum_{F\in\mathcal{F}_\mathcal{H}} (\lambda - \pi_{H,\ell}\lambda, [\![v_0]\!])_F = \sum_{F\in\mathcal{F}_\mathcal{H}} \sum_{D\in\mathcal{M}_H^F} (\lambda - \pi_{D,\ell}\lambda, [\![v_0]\!])_D = 0$$

since $[\![v_0]\!] \in \mathbb{P}_0(D)$ for all $D \in \mathcal{M}_H$, and $\pi_{D,\ell}$ is the orthogonal projection onto $\mathbb{P}_\ell(D) \supset \mathbb{P}_0(D)$. □

5. The MHM method for the Poisson problem

In this section, we revisit the convergence analysis of the MHM method using the interpolation operator introduced in Section 4. This analysis improves over the existing works [2, 4]. In particular, we obtain better constants and optimal rates in H. In addition, we are able to establish ℓ-convergence when the mesh is fixed and the polynomial degree is increased, which is new in the MHM context.

5.1. **Model problem.** Throughout this section, we fix $f \in L^2(\Omega)$ and focus on the model problem of finding $u \in H^1_0(\Omega)$ such that

$$(\boldsymbol{A}\boldsymbol{\nabla} u, \boldsymbol{\nabla} v)_\Omega = (f, v)_\Omega \qquad \forall v \in H^1_0(\Omega), \tag{5.1}$$

where, for a.e. $\boldsymbol{x}$ in Ω, $\boldsymbol{A}(\boldsymbol{x})$ is a symmetric matrix. We assume that $\boldsymbol{A}$ is measurable and that there exists two constants $0 < a_{\min} \le a_{\max} < +\infty$ such that

$$a_{\min} \le \min_{\substack{\boldsymbol{\xi}\in\mathbb{R}^d \\ |\boldsymbol{\xi}|=1}} \boldsymbol{A}(\boldsymbol{x})\boldsymbol{\xi}\cdot\boldsymbol{\xi}, \qquad \max_{\substack{\boldsymbol{\xi}\in\mathbb{R}^d \\ |\boldsymbol{\xi}|=1}} \boldsymbol{A}(\boldsymbol{x})\boldsymbol{\xi}\cdot\boldsymbol{\xi} \le a_{\max},$$

for a.e. $\boldsymbol{x}$ in Ω. For the sake of simplicity, we introduce the weighted norm

$$\|\boldsymbol{v}\|^2_{\boldsymbol{A},\mathcal{T}_\mathcal{H}} := \sum_{K\in\mathcal{T}_\mathcal{H}} \int_K \boldsymbol{A}\boldsymbol{v}\cdot\boldsymbol{v} \qquad \forall \boldsymbol{v} \in \boldsymbol{L}^2(\mathcal{T}_\mathcal{H}).$$

5.2. **MHM formulation.** Owing to Poincaré inequality, it is easily seen that the application $\|\boldsymbol{\nabla}\cdot\|_{\boldsymbol{A},\mathcal{T}_\mathcal{H}}$ is a norm over $\mathbb{P}^\perp_0(\mathcal{T}_\mathcal{H})$. We can therefore define the mappings $T : \Lambda(\partial\mathcal{T}_\mathcal{H}) \to \mathbb{P}^\perp_0(\mathcal{T}_\mathcal{H})$ and $\widehat{T} : L^2(\Omega) \to \mathbb{P}^\perp_0(\mathcal{T}_\mathcal{H})$ by requiring that

$$(\boldsymbol{A}\boldsymbol{\nabla} T(\mu), \boldsymbol{\nabla} v)_{\mathcal{T}_\mathcal{H}} = \langle \mu, v\rangle_{\partial\mathcal{T}_\mathcal{H}}, \quad (\boldsymbol{A}\boldsymbol{\nabla}\widehat{T}(g), \boldsymbol{\nabla} v)_{\mathcal{T}_\mathcal{H}} = (g, v)_{\mathcal{T}_\mathcal{H}} \quad \forall v \in \mathbb{P}^\perp_0(\mathcal{T}_\mathcal{H}), \tag{5.2}$$

for all $\mu \in \Lambda(\partial\mathcal{T}_\mathcal{H})$ and $g \in L^2(\Omega)$.

Then, the continuous MHM formulation consists of finding $(\lambda, u_0) \in \Lambda(\partial\mathcal{T}_\mathcal{H}) \times \mathbb{P}_0(\mathcal{T}_\mathcal{H})$ such that

$$\left\{ \begin{array}{rcll} \langle \mu, T(\lambda)\rangle_{\partial\mathcal{T}_\mathcal{H}} + \langle \mu, u_0\rangle_{\partial\mathcal{T}_\mathcal{H}} &=& \langle \mu, \widehat{T}(f)\rangle_{\partial\mathcal{T}_\mathcal{H}} & \forall \mu \in \Lambda(\partial\mathcal{T}_\mathcal{H}), \\ \langle \lambda, v_0\rangle_{\partial\mathcal{T}_\mathcal{H}} &=& (f, v_0)_{\mathcal{T}_\mathcal{H}} & \forall v_0 \in \mathbb{P}_0(\mathcal{T}_\mathcal{H}). \end{array} \right. \tag{5.3}$$

It is shown in [2] (see also [19]), that actually

$$\lambda|_{\partial K} = \boldsymbol{\nabla} u\cdot\boldsymbol{n}_K|_{\partial K} \qquad \text{and} \qquad u_0|_K = \frac{1}{|K|}\int_K u$$

for all $K \in \mathcal{T}_\mathcal{H}$, and that

$$u = u_0 + T(\lambda) + \widehat{T}(f). \tag{5.4}$$

Introducing the following finite dimensional subspace of $\Lambda(\partial\mathcal{T}_\mathcal{H})$

$$\Lambda_{H,\ell}(\partial\mathcal{T}_\mathcal{H}) := \left\{ \mu \in \Lambda(\partial\mathcal{T}_\mathcal{H}) \cap L^2(\partial\mathcal{T}_\mathcal{H}) \mid \mu|_D \in \mathbb{P}_\ell(D), \quad \forall D \in \mathcal{M}^F_H \ \forall F \in \mathcal{F}_\mathcal{H} \right\},$$

the discrete formulation then consists in finding $(\lambda_H, u_{0,H}) \in \Lambda_{H,\ell}(\partial\mathcal{T}_\mathcal{H}) \times \mathbb{P}_0(\mathcal{T}_\mathcal{H})$ such that

$$\left\{ \begin{array}{rcll} \langle \mu_H, T(\lambda_H)\rangle_{\partial\mathcal{T}_\mathcal{H}} + \langle \mu_H, u_{0,H}\rangle_{\partial\mathcal{T}_\mathcal{H}} &=& \langle \mu_H, \widehat{T}(f)\rangle_{\partial\mathcal{T}_\mathcal{H}} & \forall \mu_H \in \Lambda_{H,\ell}(\partial\mathcal{T}_\mathcal{H}) \\ \langle \lambda_H, v_0\rangle_{\partial\mathcal{T}_\mathcal{H}} &=& (f, v_0)_{\mathcal{T}_\mathcal{H}} & \forall v_0 \in \mathbb{P}_0(\mathcal{T}_\mathcal{H}), \end{array} \right. \tag{5.5}$$

and we set

$$u_H := u_{0,H} + T(\lambda_H) + \widehat{T}(f). \tag{5.6}$$

5.3. **Convergence analysis.** We start with a quasi-optimality result. Because the MHM formulation is a saddle point problem, Galerkin orthogonality cannot be immediately employed, and a compatibility condition is required. The approximation result follows the proof in [18, Lemma 7], but now with optimal constants.

Lemma 5.1 (Best approximation)**.** *We have*

$$\|\boldsymbol{\nabla} T(\lambda - \lambda_H)\|_{\boldsymbol{A},\mathcal{T}_\mathcal{H}} = \min_{\substack{\mu_H \in \Lambda_{H,\ell} \\ \langle \lambda - \mu_H, v_0\rangle_{\partial\mathcal{T}_\mathcal{H}} = 0 \ \forall v_0 \in \mathbb{P}_0(\mathcal{T}_\mathcal{H})}} \|\boldsymbol{\nabla} T(\lambda - \mu_H)\|_{\boldsymbol{A},\mathcal{T}_\mathcal{H}}. \tag{5.7}$$

In addition, if $\lambda \in L^2(\partial\mathcal{T}_\mathcal{H})$*, then*

$$\|\boldsymbol{\nabla} T(\lambda - \lambda_H)\|_{\boldsymbol{A},\mathcal{T}_\mathcal{H}} \le \|\boldsymbol{\nabla} T(\lambda - \pi_{H,\ell}\lambda)\|_{\boldsymbol{A},\mathcal{T}_\mathcal{H}}. \tag{5.8}$$

Proof. Consider $\mu_H \in \Lambda_{H,\ell}$ with $\langle \lambda - \mu_H, v_0\rangle_{\partial\mathcal{T}_\mathcal{H}} = 0$ for all $v_0 \in \Lambda_H$. We have

$$\begin{aligned} \|\boldsymbol{\nabla} T(\lambda - \lambda_H)\|^2_{\boldsymbol{A},\mathcal{T}_\mathcal{H}} &= (\boldsymbol{A}\boldsymbol{\nabla} T(\lambda - \lambda_H), \boldsymbol{\nabla} T(\lambda - \lambda_H))_{\mathcal{T}_\mathcal{H}} \\ &= \langle \lambda - \lambda_H, T(\lambda - \lambda_H)\rangle_{\partial\mathcal{T}_\mathcal{H}}. \end{aligned} \tag{5.9}$$

Then, using the first equations of (5.3) and (5.5), we observe that

$$\langle \mu_H, T(\lambda - \lambda_H)\rangle_{\partial\mathcal{T}_\mathcal{H}} = 0,$$

so that, from (5.9), it holds

$$\|\boldsymbol{\nabla} T(\lambda - \lambda_H)\|^2_{\boldsymbol{A},\mathcal{T}_\mathcal{H}} = \langle \lambda - \mu_H, T(\lambda - \lambda_H)\rangle_{\partial\mathcal{T}_\mathcal{H}} = (\boldsymbol{A}\boldsymbol{\nabla} T(\lambda - \mu_H), \boldsymbol{\nabla} T(\lambda - \lambda_H))_{\mathcal{T}_\mathcal{H}}.$$

Next, from the Cauchy-Schwartz inequality, we get

$$\|\boldsymbol{\nabla} T(\lambda - \lambda_H)\|_{\boldsymbol{A},\mathcal{T}_\mathcal{H}} \le \|\boldsymbol{\nabla} T(\lambda - \mu_H)\|_{\boldsymbol{A},\mathcal{T}_\mathcal{H}},$$

and (5.7) follows. Then, (5.8) follows from (4.5). □

We are now ready to establish the main result of this section.

Theorem 5.2 (Error estimate)**.** *Let* $0 \le q \le \ell$*, and* $\ell \ge 0$*, and assume that* $u \in H^{q+3}(\mathcal{P}_\Omega)$*. Then, we have*

$$\begin{aligned} &\|\boldsymbol{\nabla}(u - u_H)\|_{\mathcal{T}_\mathcal{H}} \le \\ &\qquad \mathscr{C}_{\mathcal{P}_\Omega,\mathcal{T}_\mathcal{H},q} \sqrt{\frac{a_{\max}}{a_{\min}}} \left(\frac{C_{\mathrm{A},\mathcal{M}_H,q} H}{\ell + 1}\right)^{q+3/2} \left(\mathcal{H}^{-1/2}\|u\|_{H^{q+2}(\mathcal{P}_\Omega)} + \mathcal{H}^{1/2}\|u\|_{H^{q+3}(\mathcal{P}_\Omega)}\right). \end{aligned} \tag{5.10}$$

Proof. We have

$$\|\boldsymbol{\nabla} T(\lambda - \lambda_H)\|_{\mathcal{T}_\mathcal{H}} \le a_{\min}^{-1/2} \|\boldsymbol{\nabla} T(\lambda - \lambda_H)\|_{\boldsymbol{A},\mathcal{T}_\mathcal{H}} \le a_{\min}^{-1/2} \|\boldsymbol{\nabla} T(\lambda - \pi_{H,\ell}\lambda)\|_{\boldsymbol{A},\mathcal{T}_\mathcal{H}},$$

and

$$\begin{aligned}\|\boldsymbol{\nabla} T(\lambda-\pi_{H,\ell}\lambda)\|^2_{\boldsymbol{A},\mathcal{T}_\mathcal{H}} &= \langle \lambda-\pi_{H,\ell}\lambda, T(\lambda-\pi_{H,\ell}\lambda)\rangle_{\partial\mathcal{T}_\mathcal{H}}\\ &\le \|\lambda-\pi_{H,\ell}\lambda\|_\Lambda \|\boldsymbol{\nabla} T(\lambda-\pi_{H,\ell}\lambda)\|_{\mathcal{T}_\mathcal{H}}\\ &\le a_{\max}^{1/2}\|\lambda-\pi_{H,\ell}\lambda\|_\Lambda \|\boldsymbol{\nabla} T(\lambda-\pi_{H,\ell}\lambda)\|_{\boldsymbol{A},\mathcal{T}_\mathcal{H}},\end{aligned}$$

so that

$$\|\boldsymbol{\nabla} T(\lambda-\lambda_H)\|_{\mathcal{T}_\mathcal{H}} \le \sqrt{\frac{a_{\max}}{a_{\min}}}\|\lambda-\pi_{H,\ell}\lambda\|_\Lambda.$$

Hence, (5.10) follows from (4.4). □

Remark 5.3 (Super-convergence)**.** *Under local regularity assumptions for the exact solution in the physical partition of Ω, the error estimate in Theorem 5.2 indicates that the MHM method achieves superconvergence when the skeleton diameter of the mesh H tends to zero with an additional $O(H^{1/2})$ convergence rate. Furthermore, the estimate (5.10) establishes that the MHM method provides optimally convergent solutions with respect to the degree of polynomial interpolation ℓ on the faces. These are novel results that are supported by numerical evidence presented in previous works. We also recover the (optimal) convergence classically found when $\mathcal{H}$, the diameter of the $\mathcal{T}_\mathcal{H}$ partition, vanishes. This is demonstrated by assuming the exact solution is locally regular on the physical partition, which is also new.*

6. Numerical examples

In this section, we illustrate the error estimate proved in Theorem 5.2. For this, we define the domain $\Omega = (0,1)^2$, and propose two benchmarks: First, we exhibit the convergence rates in (5.10) with respect to the parameters H and ℓ assuming the exact solution is known. Then, we consider a case of discontinuous coefficient for $\boldsymbol{A}$. We highlight the influence of the crossover interface when it coincides (or not) with an edge degree of freedom belonging to the partition skeleton. In addition, we check the accuracy of the method in relation to the contrast of coefficients in $\boldsymbol{A}$. It is worth mentioning that local problems are solved with sufficient precision so that they do not influence the error estimates.

6.1. Assessing convergence.

Consider the problem (5.1) with $\boldsymbol{A}$ the identity matrix and define $f(\boldsymbol{x}) = 8\,\pi^2\,\sin(2\,\pi\,\boldsymbol{x}_1)\,\sin(2\,\pi\,\boldsymbol{x}_2)$ such that the exact solution for (5.1) is $u(\boldsymbol{x}) = \sin(2\,\pi\,\boldsymbol{x}_1)\,\sin(2\,\pi\,\boldsymbol{x}_2)$ for all $\boldsymbol{x}\in\Omega$.

We approximate u by u_H calculated on a criss-cross mesh $\mathcal{T}_\mathcal{H}$ composed of 16 rectangular triangles. Each edge of the skeleton mesh $\mathcal{M}_\mathcal{H}$ is sequentially divided into two equal parts to define the family of approximation spaces $\{\Lambda_{H,\ell}(\partial\mathcal{T}_\mathcal{H})\}_{H,\ell>0}$, for $H = \mathcal{H}, \frac{1}{2}\mathcal{H}, \ldots, \frac{1}{32}\mathcal{H}$, and for $\ell = 0,1,2,3$. We depict in Figure 1 and Figure 2 the corresponding associated errors. From Figure 1 notice that we retrieve the super-convergence predicted in Theorem 5.2 with respect to the diameter of the skeleton mesh H. In Figure 2, we observe an exponential decay as the polynomial degree ℓ is increased. Since here the solution is analytic, this decay corresponds to the estimate (5.10) from Theorem 5.2 under the additional assumption that the constants depending on q in the estimate do not grow too fast as q increases. Notice

that since we are not able to control the growth of these aforementioned constant in terms of q, our estimate only ensures super-algebraic convergence rates for C^∞ functions. More work would be required to establish exponential convergence for analytic solutions.

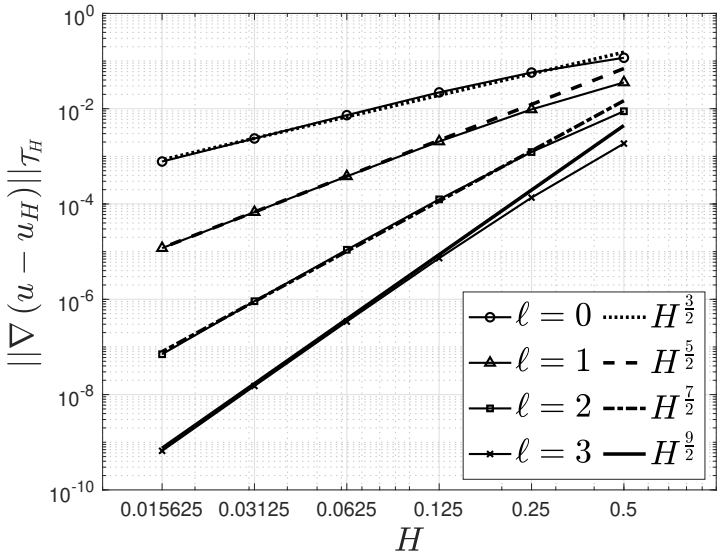

FIGURE 1. Convergence rates as a function of H for four options of ℓ. A triangular mesh of diameter $\mathcal{H} = \frac{1}{2}$ is used.

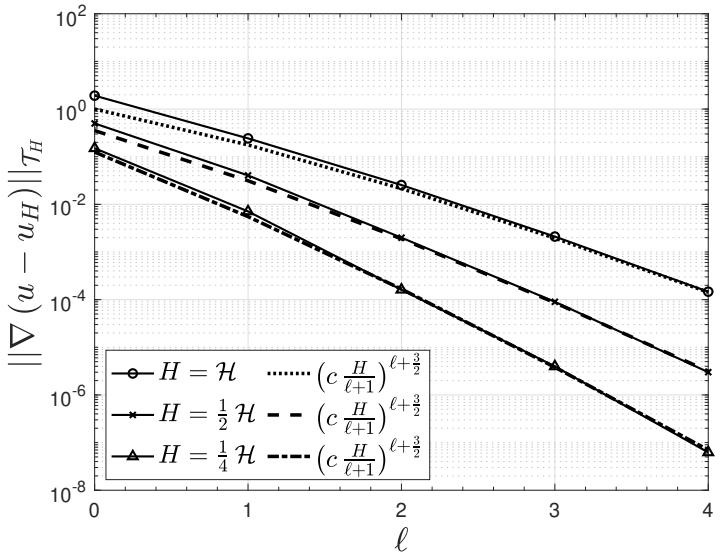

FIGURE 2. Convergence rates as a function of ℓ for three types of refinements in $\mathcal{M}_H$ (here $c = 4$).

6.2. **Assessing robustness.** We now consider problem (5.1) with $f = 1$ in Ω and $\boldsymbol{A} = a\,\mathbf{I}$, where $a : \Omega \to \mathbb{R}$ is defined by

$$a(\boldsymbol{x}) = \begin{cases} a^\star, & \text{for } \boldsymbol{x} \in (0,1) \times \left(0, \frac{1}{2}\right) \\ 1, & \text{for } \boldsymbol{x} \in (0,1) \times \left(\frac{1}{2}, 1\right) \end{cases}, \tag{6.1}$$

and $\mathbf{I}$ is the identity matrix, and $a^\star \in \mathbb{R}^+$. Since no closed formula is available for the exact solution, we consider a reference solution (still denoted by u) calculated from the standard Galerkin method on the space of continuous piecewise linear functions using a fine mesh with 1,048,576 squares that fits in the physical partition $\mathcal{P}_\Omega$.

We denote by $\mathcal{T}_\mathcal{H}^0$ the cross-mesh composed of 16 rectangular triangles with edges aligned on the jump interface. We define a family of partitions $\{\mathcal{T}_\mathcal{H}^\delta\}_{\delta>0}$ built of a perturbation of $\mathcal{T}_\mathcal{H}^0$, where δ is the parameter that measures the gap between the skeleton mesh $\mathcal{M}_\mathcal{H}^\delta$ and the physical partition $\mathcal{P}_\Omega$. We propose three scenarios for the mesh $\mathcal{T}_\mathcal{H}$, labeled S_0, S_1 and S_2 and depicted in Figure 3. In the configuration S_0, the mesh $\mathcal{T}_\mathcal{H} = \mathcal{T}_\mathcal{H}^0$ and then the edges of $\mathcal{M}_\mathcal{H}^0$ fit $\mathcal{P}_\Omega$. As for S_1, the mesh $\mathcal{T}_\mathcal{H}$ is such that the edges in $\mathcal{M}_\mathcal{H}$ are not aligned with the physical interface. In the last configuration S_2, the edges in $\mathcal{M}_\mathcal{H}$ don't fit in $\mathcal{P}_\Omega$ again, but the physical interface cuts the edges where there is a degree of freedom.

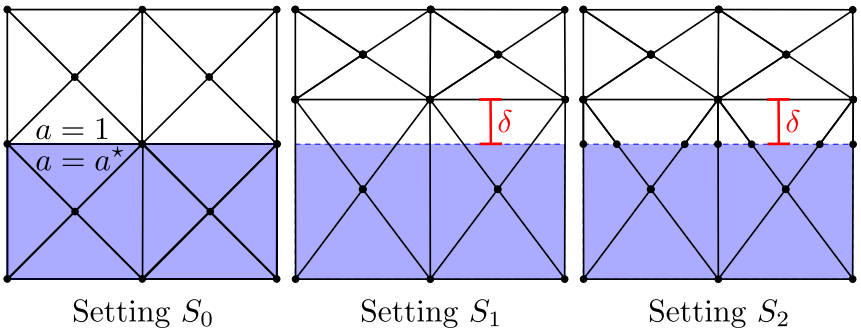

FIGURE 3. Description of three mesh settings. The black dots represent the boundaries of each edge $E \in \mathcal{M}_H$.

We studied the robustness of the MHM method in relation to δ measuring the approximation error of scenarios S_0, S_1 and S_2. Here, we set $\ell = 2$ and $a^\star = 10$, and the results are summarized in Figure 4. We observe that the error blows up when the edges are not aligned with the interface of the jump coefficient in the configuration S_1. This drawback is fully overcome by using the S_2 setting, which turns out to be equivalent to the case where the coarse mesh has aligned edges (S_0 setting). It is also interesting to note that the error is much larger in the S_1 scenario than in the S_2 one, although it decreases in the S_1 scenario when the value of δ approaches zero. The error in the S_2 scenario remains low and insensitive to the value of δ, from which we conclude that the MHM method works on meshes with small edges.

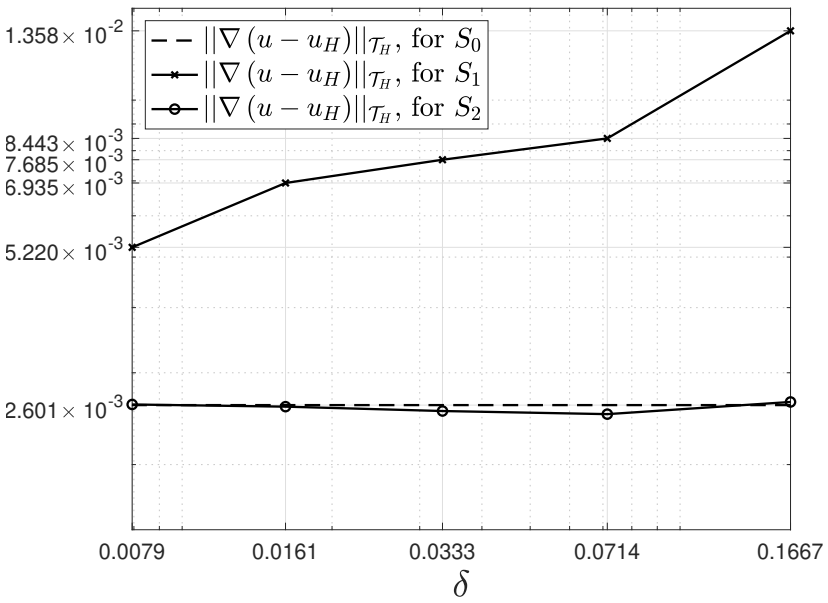

FIGURE 4. Comparison between errors in settings S_1 and S_2 when δ varies, and the error in the S_0 scenario. Here $\ell = 2$ and $a^\star = 10$.

We illustrate the elevation of u_H in Figure 5 within the different scenarios S_0, S_1 and S_2. We see that the spurious oscillation plagues the numerical solution in the configuration S_1, which is corrected by taking $\mathcal{M}_H$ such that each face in $\mathcal{M}_H$ belong to a single physical subdomain (setting S_2).

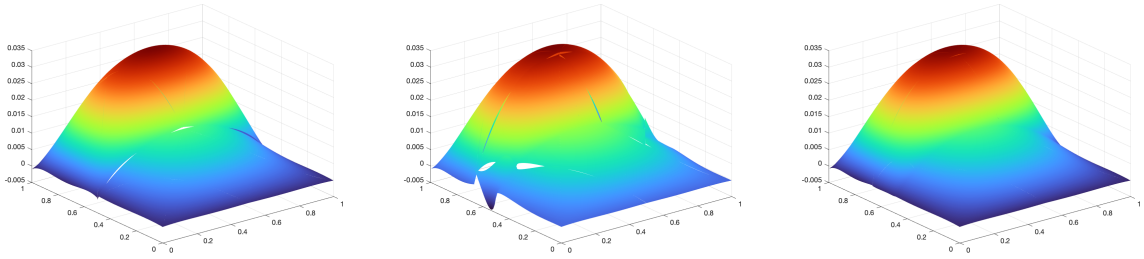

FIGURE 5. Elevation of u_H using the setting S_0 (left), S_1 (middle) and S_2 (right). Here $\delta = \frac{1}{6}$.

We also measure the error associated with the contrast $\frac{a_{\max}}{a_{\min}} = a^\star$ when changing the value of $a^\star$. We use the S_0 and S_2 settings since the S_1 scenario is not covered by Theorem 5.2. The results are summarized in Figure 6. This shows that the MHM method is less sensitive to the contrast $a^\star$ than estimated by the theory, and so (5.10) might be not sharp about the influence of contrast on error. This aspect deserves further investigation.

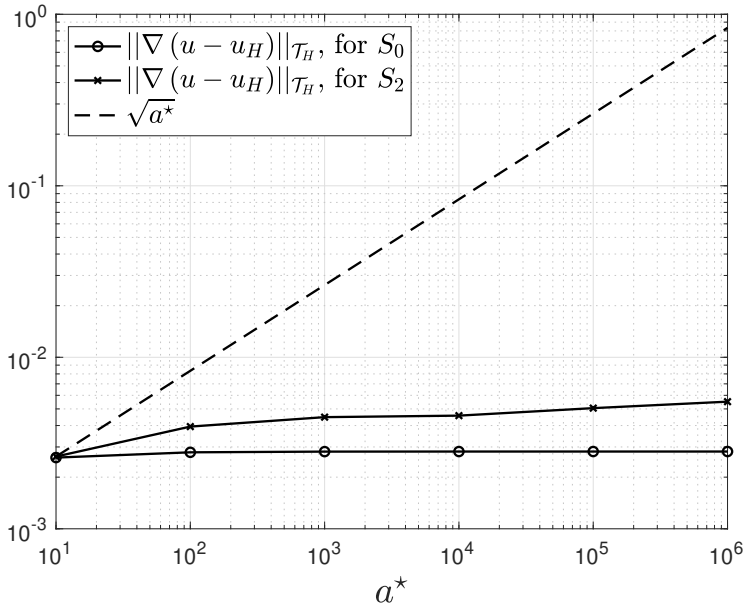

FIGURE 6. Comparison between the approximation error of the settings S_0 and S_2 with respect to contrast $a^\star$, and the theoretical rate in (5.10) given by $\sqrt{\frac{a_{\max}}{a_{\min}}} = \sqrt{a^\star}$.

7. Conclusion

We proposed a strategy to approximate fluxes in partitions not aligned with physical interfaces. Under local regularity assumptions, the theoretical result showed that the approach provides approximate fluxes with optimal convergence rates driven by exact solution regularity in physical regions. In other words, we replace the restrictive assumption about the regularity of the exact solution in each mesh element with the regularity of the solution in physical regions. In addition, we highlight the dependence of the constant on the polynomial degree used to approximate the exact fluxes.

We leverage these findings to improve the convergence results for the MHM method applied to the Poisson problem. We mainly prove that the MHM method is super-convergent on non-aligned meshes, assuming exact solution regularity only in the physical partition. Such mathematical analysis supports the numerical evidence originally anticipated in [13]. It is worth mentioning that the results can be easily extended to MHM methods applied to other operators such as the linear elasticity model or the reactive-advective-diffusive equation, for example. Furthermore, the discrete flux can be exploited in other flux-based numerical methods or domain decomposition techniques and inherit from its properties.

References

[1] R. A. Adams. *Sobolev spaces*. Academic Press, 1975.

[2] R. Araya, C. Harder, D. Paredes, and F. Valentin. Multiscale hybrid-mixed method. *SIAM J. Numer. Anal.*, 51(6):3505–3531, 2013.
[3] G.R. Barrenechea and F. Chouly. A local projection stabilized method for fictitious domains. *Applied Mathematics Letters*, 25:2071–2076, 2012.
[4] G.R. Barrenechea, F. Jaillet, D. Paredes, and F. Valentin. The multiscale hybrid mixed method in general polygonal meshes. *Numer. Math.*, 145:197–237, 2020.
[5] S. Bertoluzza. Local boundary estimates for the lagrange multiplier discretization of a dirichlet boundary value problem with application to domain decomposition. *Calcolo*, 43:121–149, 2006.
[6] E. Burman, S. Claus, P. Hansbo, M. Larson, and A. Massing. Cutfem: Discretizing geometry and partial differential equations. *Int. J. Numer. Meth. Engng.*, 104:472–501, 2015.
[7] A. Cangiani, Z. Dong, E.H. Georgoulis, and P. Houston. *hp-version discontinuous Galerkin methods on polygonal and polyhedral meshes*. Springer, 2017.
[8] T. Chaumont-Frelet, A. Ern, S. Lemaire, and F. Valentin. Bridging the multiscale hybrid-mixed and multiscale hybrid high-order methods. *ESAIM: M2AN*, 56(1):261–285, 2022.
[9] L. Beirão de Veiga, A. Chernov, L. Mascotto, and A. Russo. Basic principles of *hp* virtual elements on quasiuniform meshes. *Math. Models Methods Appl. Sci.*, 26(8):1567–1598, 2016.
[10] L. Beirão de Veiga, C. Lovadina, and A. Russo. Stability analysis for the virtual element method. *Math. Models Methods Appl. Sci.*, 27(13):2557–2594, 2017.
[11] V. Girault and P.A. Raviart. *Finite Element Methods for Navier-Stokes Equations: Theory and Algorithms*, volume 5 of *Springer Series in Computational Mathematics*. Springer-Verlag, Berlin, New-York, 1986.
[12] C. Harder, D. Paredes, and F. Valentin. A family of multiscale hybrid-mixed finite element methods for the Darcy equation with rough coefficients. *J. Comput. Phys.*, 245:107–130, 2013.
[13] C. Harder, D. Paredes, and F. Valentin. On a multiscale hybrid-mixed method for advective-reactive dominated problems with heterogenous coefficients. *SIAM Multiscale Model. and Simul.*, 13(2):491–518, 2015.
[14] C. Harder and F. Valentin. Foundations of the MHM method. In G. R. Barrenechea, F. Brezzi, A. Cangiani, and E. H. Georgoulis, editors, *Building Bridges: Connections and Challenges in Modern Approaches to Numerical Partial Differential Equations*, Lecture Notes in Computational Science and Engineering. Springer, 2016.
[15] C. Kim, R.D. Lazarov, J.E. Pasciak, and P.S. Vassilevski. Multiplier spaces for the mortar finite element method in three dimensions. *SIAM J. Numer. Anal.*, 39(2):519–538, 2001.
[16] M. G. Larson and A. Massing. L^2-error estimates for finite element approximations of boundary fluxes. 2014.
[17] J. M. Melenk and B. Wohlmuth. Quasi-optimal approximation of surface based lagrange multipliers in finite element methods. *SIAM J. Numer. Anal.*, 50(4):2064–2087, 2012.
[18] D. Paredes, F. Valentin, and H. M. Versieux. On the robustness of multiscale hybrid-mixed methods. *Math. Comp.*, 86(304):525–548, 2017.
[19] P.A. Raviart and J.M. Thomas. Primal hybrid finite element methods for 2nd order elliptic equations. *Math. Comp.*, 31(138):391–413, 1977.
[20] E.M. Stein. *Singular integrals and differentiability properties of functions*. Priceton university press, 1970.
[21] L. Tartar. *An introduction to Sobolev spaces and interpolation spaces*. Springer, 2007.

Centro de Investigación en Ingeniería Matemática (CI^{2}MA)

PRE-PUBLICACIONES 2022 - 2023

2022-28 Jorge Albella, Rodolfo Rodríguez, Pablo Venegas: *Numerical approximation of a potentials formulation for the elasticity vibration problem*

2022-29 Liliana Camargo, Bibiana López-Rodríguez, Mauricio Osorio, Manuel Solano: *An adaptive and quasi-periodic HDG method for Maxwell's equations in heterogeneous media*

2022-30 Gabriel N. Gatica, Nicolas Nuñez, Ricardo Ruiz-Baier: *Mixed-primal methods for natural convection driven phase change with Navier-Stokes-Brinkman equations*

2022-31 Diego Paredes, Frederic Valentin, Henrique M. Versieux: *Revisiting the robustness of the multiscale hybrid-mixed method: the face-based strategy*

2022-32 Franz Chouly, Tom Gustafsson, Patrick Hild: *A Nitsche method for the elastoplastic torsion problem*

2022-33 Olusegun Adebayo, Stéphane P. A. Bordas, Franz Chouly, Raluca Eftimie, Gwenaël Rolin, Stéphane Urcun: *Modelling Keloids Dynamics: A Brief Review and New Mathematical Perspectives*

2022-34 Nicolás Carro, David Mora, Jesús Vellojín: *A finite element model for concentration polarization and osmotic effects in a membrane channel*

2022-35 Claudio I. Correa, Gabriel N. Gatica, Esteban Henriquez, Ricardo Ruiz-Baier, Manuel Solano: *Banach spaces-based mixed finite element methods for the coupled Navier–Stokes and Poisson–Nernst–Planck equations*

2022-36 Gabriel R. Barrenechea, Antonio Tadeu A. Gomes, Diego Paredes: *A Multiscale Hybrid Method*

2022-37 Rodrigo Abarca Del Rio, Fernando Campos, Dieter Issler, Mauricio Sepúlveda: *Study of Avalanche Models Using Well Balanced Finite Volume Schemes*

2023-01 Julio Careaga, Gabriel N. Gatica: *Coupled mixed finite element and finite volume methods for a solid velocity-based model of multidimensional settling*

2023-02 Theophile Chaumont Frelet, Diego Paredes, Frederic Valentin: *Flux approximation on unfitted meshes and application to multiscale hybrid-mixed methods*

Para obtener copias de las Pre-Publicaciones, escribir o llamar a: Director, Centro de Investigación en Ingeniería Matemática, Universidad de Concepción, Casilla 160-C, Concepción, Chile, Tel.: 41-2661324, o bien, visitar la página web del centro: http://www.ci2ma.udec.cl







Centro de Investigación en
Ingeniería Matemática (CI²MA)
Universidad de Concepción

Casilla 160-C, Concepción, Chile
Tel.: 56-41-2661324/2661554/2661316
http://www.ci2ma.udec.cl